

# MultiMAE for Brain MRIs: Robustness to Missing Inputs Using Multi-Modal Masked Autoencoder

Ayhan Can Erdur<sup>1,2,\*</sup>, Christian Beischl<sup>2,\*</sup>, Daniel Scholz<sup>2,3,4</sup>, Jiazen Pan<sup>2</sup>,  
Benedikt Wiestler<sup>3,4,•</sup>, Daniel Rueckert<sup>2,4,5,•</sup>, and Jan C. Peek<sup>1,6,7,•</sup>

<sup>1</sup> Department of Radiation Oncology, TUM University Hospital, Munich, Germany

<sup>2</sup> Chair for AI in Healthcare and Medicine, Technical University of Munich (TUM)  
and TUM University Hospital, Munich, Germany

<sup>3</sup> Chair for AI for Image-Guided Diagnosis and Therapy, Technical University of  
Munich (TUM) and TUM University Hospital, Munich, Germany

<sup>4</sup> Munich Center for Machine Learning (MCML), Munich, Germany

<sup>5</sup> Department of Computing, Imperial College London, London, UK

<sup>6</sup> Deutsches Konsortium für Translationale Krebsforschung (DKTK), Partner Site  
Munich, Munich, Germany

<sup>7</sup> Institute of Radiation Medicine (IRM), Department of Radiation Sciences (DRS),  
Helmholtz Center Munich, Munich, Germany

\* contributed equally as first authors, • contributed equally as last authors  
can.erdur@tum.de

**Abstract.** Missing input sequences are common in medical imaging data, posing a challenge for deep learning models reliant on complete input data. In this work, inspired by MultiMAE [2], we develop a masked autoencoder (MAE) paradigm for multi-modal, multi-task learning in 3D medical imaging with brain MRIs. Our method treats each MRI sequence as a separate input modality, leveraging a late-fusion-style transformer encoder to integrate multi-sequence information (“multi-modal”) and individual decoder streams for each modality for “multi-task” reconstruction. This pretraining strategy guides the model to learn rich representations per modality while also equipping it to handle missing inputs through cross-sequence reasoning. The result is a flexible and generalizable encoder for brain MRIs that infers missing sequences from available inputs and can be adapted to various downstream applications. We demonstrate the performance and robustness of our method against an MAE-ViT baseline in downstream segmentation and classification tasks, showing absolute improvement of 10.1 overall Dice score and 0.46 MCC over the baselines with missing input sequences. Our experiments demonstrate the strength of this pretraining strategy. The implementation is made available<sup>8</sup>.

**Keywords:** Masked Autoencoder Pretraining · Brain MRI · Missing Modalities

---

<sup>8</sup> The repository for our work: <https://github.com/chris-beischl/multimae-for-brain-mri>

## 1 Introduction

Pretraining has become a cornerstone of modern deep learning, particularly in data-scarce domains like medical imaging, where labeled annotations are costly and limited. Self-supervised learning offers an effective solution, enabling models to learn transferable representations from unlabeled scans and consistently outperform training from scratch [1,18,26]. The basis for the self-supervised learning strategy is the use of a pretext task, such as the reconstruction of masked parts of the inputs [9].

Transformer-based architectures have rapidly gained traction in medical imaging, both as pure Vision Transformers (ViTs) [7] and in hybrid CNN-transformer designs, showing strong performance in classification [6,11], and segmentation [8,10].

Despite architectural differences, there is one common approach adopted by most of the existing work with magnetic resonance imaging (MRI): processing multiple modalities by stacking them along the channel dimension, analogous to RGB channels in natural images [8,10]. While this early-fusion strategy is simple, it requires all modalities to be present during training and inference, which very often is not the case in real-life clinical environments. Moreover, it limits modality-specific representation learning and leads to sharp performance drops when inputs are missing [27].

In this work, we adopt a MultiMAE-based [2] pretraining framework with modality-specific encoding to strengthen the learning of distinct representations per sequence and their cross-modal integration, rather than treating all inputs as a single fused whole from the outset, and masked modeling to improve robustness to missing modalities. This approach introduces only minor changes to the ViT backbone and outperforms standard MAE [9] pretraining in both segmentation and classification, particularly under missing-modality conditions. Our key contributions are as follows:

1. We investigate MultiMAE pretraining for 3D brain MRI, enabling modality-specific encoding and masked modeling across multiple MRI sequences.
2. We show that **pretraining improves performance and robustness to missing input modalities** in both segmentation (glioma, metastasis) and classification of glioma subtypes into glioblastoma (GBM), astrocytoma (Astro), and oligodendrogioma (Oligo) according to WHO 2021 standards. The improvement is evident both in internal and external test sets.
3. We demonstrate that MultiMAE can **synthesize entirely missing modalities** at inference time.

## 2 Related Work

**Self-Supervised and Multi-Modal Learning in Medical Imaging** Medical image analysis often suffers from scarce annotated data due to the high cost and effort of expert labeling [20,1]. Self-supervised learning (SSL) addresses this by

leveraging large unlabeled datasets to boost downstream task performance, a strategy increasingly adopted in medical imaging [28,20].

SSL approaches include generative methods like masked autoencoding [26], discriminative contrastive learning [1,5], and hybrid objectives combining both [28,20]. Masked autoencoders (MAEs) [9] have been extended to 3D medical data, with MAE-UNETR [26] demonstrating notable gains in segmentation.

**Handling Missing Modalities and Robustness** Multi-modal learning leverages complementary data sources, such as images and text [23], or different imaging acquisitions. Typically, models use modality-specific encoders with fusion layers to capture cross-modal interactions. Besides performance benefits, such fusion improves robustness to missing modalities [25,22].

For natural images, MultiMAE [2] offers a simple and versatile multi-modal SSL to learn joint representations across imaging modalities. It remains, however, underexplored in medical imaging.

### 3 Materials and Methods

#### 3.1 Dataset

We use the 2021 edition of BraTS Glioma [12], along with the UPENN-GBM [3], UCSF-PGDM [4], Lumiere [19], Rembrandt [16], EGD [21], TCGA [24], and the 2023 edition of the BraTS Metastasis dataset [13]. Patient overlaps between BraTS’21 and other sources are removed. The combined dataset is randomly split for pretraining as 3243/650/434 (train/val/test). For out-of-distribution, external evaluation, we additionally use in-house datasets comprising 252 glioma and 167 brain metastasis cases.

Each downstream dataset is refined to exclude irrelevant or postoperative scans. Glioma segmentation uses 2676/536/358 + 252, metastasis segmentation 567/114/76 + 167, and subtype classification 1253/251/168 + 203 patients, with GBM/Astro/Oligo prevalence of 80/13/7% internally and 77/12/11% externally.

All four MRI sequences (t1, t1c, t2, fla) are skull-stripped, resampled to 1mm<sup>3</sup> isotropic resolution, and registered to the SRI24 atlas [14]. Expert-made segmentations following the BraTS convention are available for all patients, except for the external metastasis dataset, which lacks enhancing tumor labels.

#### 3.2 Model Architecture and Pretraining

We adopt the MultiMAE [2] framework using a modified ViT, which encodes shared representations across multiple imaging modalities as our backbone.

Non-overlapping 16 × 16 × 16 patches from each modality are projected into a shared token space via modality-specific linear adapters. A global masking ratio is set as 75%, with per-modality masking sampled from a Dirichlet distribution ( $\alpha = 1$ ), allowing up to 100% masking of a modality while preserving the expected global rate. Unmasked tokens from all modalities, along with a [cls] token, form the input sequence.

Each modality is reconstructed using a dedicated output transformer. For masked patches, learnable [mask] tokens are inserted at their original positions to form the query sequence. As in [2], the decoders are implemented as *cross-attention transformers*: queries first attend to the context via a single cross-attention layer, followed by standard self-attention layers. The modality-specific masking scheme encourages each decoder to reconstruct missing patches using both its visible tokens and the shared multi-modal context, enabling the model to capture rich cross-modal dependencies during training.

Following prior work [9,2,26], we adopt an asymmetric encoder-decoder design. The encoder is a ViT-B/16 architecture (12 layers; token size:  $t \in \mathbb{R}^{768}$ ; 12 attention heads). The modality-specific decoders are lightweight (3 layers;  $t \in \mathbb{R}^{384}$ ; 12 heads). Both the encoder and decoders use 3D sine-cosine positional embeddings.

The pretraining optimizes reconstruction using an MSE loss over all tokens. To reduce redundancy from background-only regions and maintain compatibility with the patch size, we crop inputs to  $160 \times 176 \times 144$  around the foreground.

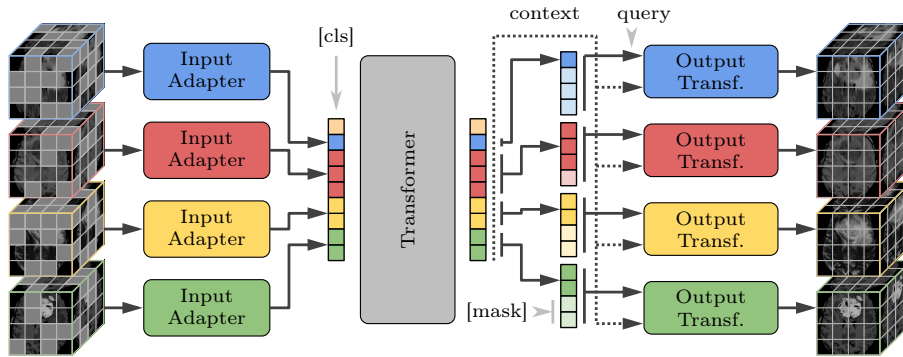


Fig. 1. Adapting the MultiMAE workflow for brain MRIs

### 3.3 Adaptation to Downstream Tasks

**Segmentation** We use the UNETR [26] architecture for its off-the-shelf applicability without modifications to the ViT encoder. It performs segmentation via convolutional upsampling of patch tokens from different encoder layers, similar to skip connections of U-Net [15]. However, it expects a fixed-length token sequence for spatial consistency. Since each input modality is tokenized separately in our method, the sequence length is variable. We maintain a consistent length by averaging the tokens at each spatial location.

We randomly crop the MRI sequences into  $128 \times 128 \times 128$  during finetuning. At test time, shape consistency is achieved through sliding window inference with a 25% overlap. The model is optimized using the Dice loss.

**Classification** For classification, the decoders are replaced with a single linear layer  $\mathbb{R}^{768 \times 3}$ . To aggregate the patch tokens into a single feature vector, we average them together with the CLS token.

We finetune the network with cross-entropy loss. The minority classes, Oligo and Astro, are oversampled to match a uniform distribution with GBM, mitigating the common class imbalance in medical imaging [17].

### 3.4 Evaluation

For each downstream task, we train a vanilla ViT-B/16 baseline that handles multi-modal MRIs through stacking along the channel dimension. Following [26], we perform a MAE pretraining for this ViT with the same masking ratio and decoder configuration as in their work (8 layers; token size:  $t \in \mathbb{R}^{384}$ ; 12 heads).

We monitor the effectiveness of pretraining and the thus achieved MRI generation via PSNR and SSIM. Segmentation is evaluated using the Dice score on enhancing tumor (ET), tumor core (TC), and whole tumor (WT), per BraTS guidelines. For classification tasks, we report the multi-class accuracy, F1 score, and Matthew’s correlation coefficient (MCC).

All four MRI sequences are provided during finetuning. At test time, we evaluate five scenarios: one with all inputs and four with a single modality removed. Tables in section 4 depict these scenarios. For our model, the missing modality is simply excluded, while for the vanilla ViT, it is filled with background intensities due to the fixed input shape. No masking is applied during finetuning, making this a truly *unprepared* setting for evaluating robustness to unseen input configurations.

### 3.5 Training Setup

All pretrainings run for 1200 epochs with a batch size of 16. Downstream finetunings and their from-scratch counterparts are performed for 100 epochs. Classification uses the same batch size, while segmentation is limited to two due to memory constraints (NVIDIA A40 GPUs). We use the AdamW optimizer with a learning rate of  $1e-4$  and 0.05 weight decay. During MAE pretrainings, the learning rate is rescaled by 0.1 on a plateau of 50 epochs. For downstream tasks, we apply cosine decay with 40 warmup epochs. A gradient clipping by 0.5 is applied in all settings.

## 4 Results

### 4.1 Missing MRI Generation

The multi-task MAE pretraining naturally enables image generation, treating the missing modality as a fully masked input. The encoder-decoder structure leverages its cross-modal capabilities to generate the missing input based on the three present inputs.

As shown in Table 1 and Figure 2, the model produces anatomically realistic outputs, though some blurring and loss of fine detail remain. In contrast, the vanilla ViT fails to achieve comparable reconstruction quality, even after pretraining.

**Table 1.** MRI sequence generation performance. Each column reports the reconstruction quality (PSNR and SSIM) for the "missing" MRI sequence, generated from the remaining three modalities. A ViT pretrained with MAE is shown for comparison.

Backbone	PSNR				SSIM			
	t1	t1c	t2	fla	t1	t1c	t2	fla
ViT	7.36	8.18	10.36	8.01	0.52	0.54	0.61	0.55
ours	<b>21.58</b>	<b>20.56</b>	<b>21.01</b>	<b>20.74</b>	<b>0.76</b>	<b>0.71</b>	<b>0.71</b>	<b>0.71</b>

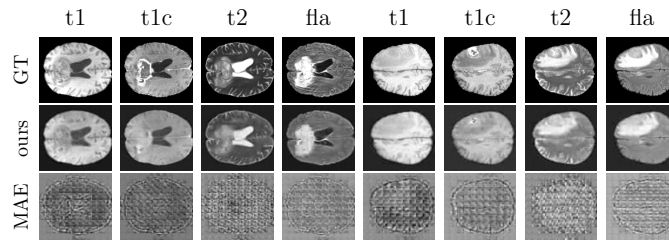


**Fig. 2. Reconstruction of a missing modality.** The depicted modality was fully masked (for MAE: replaced with background), and then reconstructed using the remaining inputs.

## 4.2 Segmentation

As shown in Table 2 and Table 3, our pretrained model consistently outperforms the MAE-ViT baseline, both on internal and external datasets. Despite using a frozen encoder in finetuning for simplicity, it achieves on-par performance, indicating the effectiveness of the learned representations. On the more underexplored task of metastasis segmentation, Table 3 highlights the value of our pretraining; there is substantial improvement compared to training *from scratch* (randomly initialized).

In missing modality experiments, our method proves far more robust than ViT. Performance patterns align with clinical expectations, e.g., t1 and t1c are more predictive for ET and TC, while WT depends more on FLAIR, showing that our model learns to leverage the most relevant inputs, whereas ViT suffers higher performance drops overall, even when key modalities are not missing.

**Table 2. Glioma segmentation (Internal + External).** Dice scores for ViT and our pretrained model on internal and external test sets. We report performance for tumor core (TC), enhancing tumor (ET), and whole tumor (WT) under three training regimes: scratch, frozen (internal), and frozen (external).

Modalities	Enc.	TC			ET			WT		
		scr.		frozen	scr.	frozen	scr.	frozen	scr.	frozen
		int.	int.	ext.	int.	int.	ext.	int.	int.	ext.
✓ ✓ ✓ ✓	ViT	73.75	74.30	<b>67.90</b>	71.00	72.33	66.43	81.48	80.40	74.73
	ours	72.36	<b>75.15</b>	65.75	71.07	<b>73.00</b>	<b>66.84</b>	80.73	<b>82.78</b>	<b>78.80</b>
✗ ✓ ✓ ✓	ViT	22.07	47.91	30.93	21.16	45.76	38.19	25.66	47.85	48.61
	ours	8.11	<b>51.55</b>	<b>45.00</b>	6.95	<b>48.96</b>	<b>49.80</b>	19.44	<b>79.03</b>	<b>76.54</b>
✓ ✗ ✓ ✓	ViT	25.32	21.55	25.07	6.99	7.23	12.56	41.77	64.98	55.91
	ours	13.64	<b>37.85</b>	<b>32.90</b>	<b>7.46</b>	<b>7.46</b>	<b>12.81</b>	53.58	<b>80.08</b>	<b>76.59</b>
✓ ✓ ✗ ✓	ViT	50.04	64.86	49.34	60.72	64.98	50.98	55.71	<b>64.00</b>	<b>44.64</b>
	ours	28.81	<b>66.72</b>	<b>60.14</b>	57.07	<b>69.30</b>	<b>62.75</b>	25.83	53.55	36.34
✓ ✓ ✓ ✗	ViT	0.74	14.42	18.96	2.03	17.00	22.65	0.05	5.29	4.31
	ours	16.88	<b>38.91</b>	<b>30.95</b>	15.50	<b>37.11</b>	<b>34.96</b>	7.63	<b>16.69</b>	<b>10.12</b>

**Table 3. Metastasis Segmentation (Internal + External)** Enhancing tumor (ET) labels are not available for the external test set.

Modalities	Enc.	TC			ET			WT		
		scr.		frozen	scr.	frozen	scr.	frozen	scr.	frozen
		int.	int.	ext.	int.	int.	int.	int.	int.	ext.
✓ ✓ ✓ ✓	ViT	38.40	42.19	33.39	40.87	37.58	53.76	54.61	48.55	
	ours	15.28	<b>58.19</b>	<b>51.67</b>	16.76	<b>63.48</b>	31.71	<b>75.07</b>	<b>63.24</b>	
✗ ✓ ✓ ✓	ViT	23.71	16.98	5.61	18.34	8.55	25.74	22.91	14.63	
	ours	1.17	<b>46.43</b>	<b>31.22</b>	0.73	<b>35.08</b>	3.19	<b>66.92</b>	<b>58.45</b>	
✓ ✗ ✓ ✓	ViT	0.71	2.33	4.86	1.55	6.61	24.93	58.70	46.40	
	ours	<b>2.98</b>	1.72	<b>6.29</b>	1.49	<b>7.46</b>	24.24	<b>72.89</b>	<b>62.93</b>	
✓ ✓ ✗ ✓	ViT	8.57	13.93	21.69	14.70	4.72	3.34	18.05	<b>33.68</b>	
	ours	8.41	<b>38.21</b>	<b>35.87</b>	9.50	<b>47.39</b>	9.93	<b>21.17</b>	12.13	
✓ ✓ ✓ ✗	ViT	2.96	1.82	5.08	3.51	5.51	5.16	0.10	0.04	
	ours	0.88	<b>30.58</b>	<b>17.59</b>	1.06	<b>31.64</b>	0.12	<b>8.77</b>	<b>3.98</b>	

### 4.3 Classification

In the multi-class glioma subtyping task, a similar trend to segmentation is observed: our pretrained model consistently outperforms the MAE-ViT baseline across both internal (Table 4) and external (Table 5) datasets. It achieves strong performance, with MCC scores reaching up to 0.70. Remarkably, this performance is largely retained even when one modality is missing, whereas the ViT baseline shows a more substantial drop. A moderate decline is only observed in the absence of t1c, which is expected due to its critical role in characterizing tumor enhancement.

In contrast to segmentation, freezing the encoder during finetuning is less effective for classification, likely because a single linear layer is insufficient to align the learned representations with the task. This limitation is also evident for the vanilla ViT. However, full finetuning, which is more feasible here due to the model size, boosts performance.

**Table 4. Glioma Subtype Classification (Internal)** All metrics are computed for the multi-class setting.

Modalities	Enc.	Accuracy			F1			MCC		
		scr.	frozen	full	scr.	frozen	full	scr.	frozen	full
✓ ✓ ✓ ✓	ViT	0.85	0.67	0.89	0.67	0.49	0.63	0.59	0.39	0.66
	ours	0.73	0.68	<b>0.90</b>	0.54	0.49	<b>0.73</b>	0.43	0.38	<b>0.69</b>
✗ ✓ ✓ ✓	ViT	0.51	0.13	0.41	0.35	0.08	0.26	0.15	0.00	0.03
	ours	0.61	0.71	<b>0.89</b>	0.46	0.49	<b>0.70</b>	0.31	0.36	<b>0.66</b>
✓ ✗ ✓ ✓	ViT	0.25	0.70	0.06	0.17	0.41	0.04	0.12	0.22	-0.10
	ours	0.67	0.47	<b>0.79</b>	0.46	0.36	<b>0.66</b>	0.27	0.20	<b>0.47</b>
✓ ✓ ✗ ✓	ViT	0.58	0.13	0.75	0.37	0.08	0.43	0.36	0.0	0.36
	ours	0.5	0.76	<b>0.89</b>	0.40	0.53	<b>0.66</b>	0.31	0.40	<b>0.66</b>
✓ ✓ ✓ ✗	ViT	0.45	0.78	0.81	0.30	0.41	0.46	0.13	0.17	0.37
	ours	0.81	0.64	<b>0.91</b>	0.50	0.46	<b>0.74</b>	0.41	0.35	<b>0.71</b>

**Table 5. Glioma Subtype Classification (External)** Results are shown only for the fully finetuned model.

Metric	all		no-t1		no-t1c		no-t2		no-fla	
	ViT	ours	ViT	ours	ViT	ours	ViT	ours	ViT	ours
Accuracy	0.78	<b>0.79</b>	0.37	<b>0.80</b>	0.12	<b>0.49</b>	0.73	<b>0.79</b>	0.75	<b>0.78</b>
F1	0.47	<b>0.48</b>	0.25	<b>0.46</b>	0.10	<b>0.36</b>	0.43	<b>0.48</b>	0.36	<b>0.46</b>
MCC	<b>0.39</b>	0.36	0.11	<b>0.38</b>	0.06	<b>0.12</b>	0.36	<b>0.39</b>	0.15	<b>0.33</b>

## 5 Conclusion

In this work, we present a MultiMAE pretraining framework for 3D brain MRI using masked modeling across multiple sequences and modality-specific encoding. Unlike early-fusion methods that treat all modalities as a single block, our approach learns distinct yet complementary representations per sequence, enhancing robustness to missing inputs common in clinical practice.

Our pretrained model consistently outperforms a baseline MAE-ViT in both segmentation and classification, showing strong performance on internal data and good generalization externally. However, a domain gap persists, reflecting the common challenge of adapting across clinical sites in medical imaging.

Particularly notable is the model’s resilience to missing modalities: it continues to perform competitively even when an entire input sequence is absent, and is capable of extracting the information through learned cross-modal relationships. This is further evidenced by the model’s strong ability to synthesize a missing modality from the remaining three. Still, the reconstructions show some blurring and loss of fine details, likely due to the limitations of pixel-wise MSE loss. Future work could address this by exploring perceptual or feature-level loss functions to enhance reconstruction fidelity.

Nonetheless, our approach shows greater dependence on pretraining compared to a vanilla ViT, with randomly initialized versions yielding weaker performance in some cases. This likely suggests that the added complexity of cross-modal integration demands more data or longer training to converge effectively. While pretraining requires considerable compute, it is performed only once and with minimal additional cost, can then be flexibly adapted to diverse tasks and resource-constrained environments.

Finally, the downstream performance is ultimately bounded by the used decoders; future gains may come from more advanced decoding strategies.

In conclusion, we present a simple yet effective reformulation of MAE pre-training paradigm that enables more elegant handling of multi-modal brain MRI data.

**Acknowledgments.** This study was supported by the DFG, grant #504320104.

**Disclosure of Interests.** The authors have no competing interests to declare that are relevant to the content of this article.

## References

1. Azizi, S., Mustafa, B., Ryan, F., Beaver, Z., Freyberg, J., Deaton, J., Loh, A., et al.: Big self-supervised models advance medical image classification. In: Proceedings of the IEEE/CVF international conference on computer vision. pp. 3478–3488 (2021)
2. Bachmann, R., Mizrahi, D., Atanov, A., Zamir, A.: Multimae: Multi-modal multi-task masked autoencoders. In: European Conference on Computer Vision. pp. 348–367. Springer (2022)
3. Bakas, S., Sako, C., Akbari, H., Bilello, M., Sotiras, A., Shukla, G., et al.: The university of pennsylvania glioblastoma (upenn-gbm) cohort: advanced mri, clinical, genomics, & radiomics. *Scientific data* **9**(1), 453 (2022)
4. Calabrese, E., Villanueva-Meyer, J.E., Rudie, J.D., Rauschecker, A.M., Baid, U., Bakas, S., et al.: The university of california san francisco preoperative diffuse glioma mri dataset. *Radiology: Artificial Intelligence* **4**(6), e220058 (2022)
5. Chaitanya, K., Erdil, E., Karani, N., Konukoglu, E.: Contrastive learning of global and local features for medical image segmentation with limited annotations. *Advances in neural information processing systems* **33**, 12546–12558 (2020)
6. Dai, Y., Gao, Y., Liu, F.: Transmed: Transformers advance multi-modal medical image classification. *Diagnostics* **11**(8), 1384 (2021)

7. Dosovitskiy, A., Beyer, L., Kolesnikov, A., Weissenborn, D., Zhai, X., Unterthiner, T., et al.: An image is worth 16x16 words: Transformers for image recognition at scale. In: 9th International Conference on Learning Representations, ICLR 2021 (2021)
8. Hatamizadeh, A., Tang, Y., Nath, V., Yang, D., Myronenko, A., Landman, B., et al.: Unetr: Transformers for 3d medical image segmentation. In: Proceedings of the IEEE/CVF winter conference on applications of computer vision. pp. 574–584 (2022)
9. He, K., Chen, X., Xie, S., Li, Y., Dollár, P., Girshick, R.: Masked autoencoders are scalable vision learners. In: Proceedings of the IEEE/CVF conference on computer vision and pattern recognition. pp. 16000–16009 (2022)
10. Jiang, Y., Zhang, Y., Lin, X., Dong, J., Cheng, T., Liang, J.: Swinbts: A method for 3d multimodal brain tumor segmentation using swin transformer. *Brain sciences* **12**(6), 797 (2022)
11. Manzari, O.N., Ahmadabadi, H., Kashiani, H., Shokouhi, S.B., Ayatollahi, A.: Medvit: a robust vision transformer for generalized medical image classification. *Computers in biology and medicine* **157**, 106791 (2023)
12. Menze, B.H., Jakab, A., Bauer, S., Kalpathy-Cramer, J., Farahani, K., Kirby, J., et al.: The multimodal brain tumor image segmentation benchmark (brats). *IEEE transactions on medical imaging* **34**(10), 1993–2024 (2014)
13. Moawad, A.W., Janas, A., Baid, U., Ramakrishnan, D., Saluja, R., Ashraf, N., et al.: The brain tumor segmentation-metastases (brats-mets) challenge 2023: Brain metastasis segmentation on pre-treatment mri. *ArXiv* pp. arXiv–2306 (2024)
14. Rohlfing, T., Zahr, N.M., Sullivan, E.V., Pfefferbaum, A.: The sri24 multichannel atlas of normal adult human brain structure. *Human brain mapping* **31**(5), 798–819 (2010)
15. Ronneberger, O., Fischer, P., Brox, T.: U-net: Convolutional networks for biomedical image segmentation. In: Medical image computing and computer-assisted intervention–MICCAI 2015: 18th international conference, Munich, Germany, October 5-9, 2015, proceedings, part III 18. pp. 234–241. Springer (2015)
16. Sayah, A., Bencheqroun, C., Bhuvaneshwar, K., Belouali, A., Bakas, S., Sako, C., et al.: Enhancing the rembrandt mri collection with expert segmentation labels and quantitative radiomic features. *Scientific Data* **9**(1), 338 (2022)
17. Scholz, D., Erdur, A.C., Buchner, J.A., Peeken, J.C., Rueckert, D., Wiestler, B.: Imbalance-aware loss functions improve medical image classification. *Medical imaging with deep learning* pp. 1341–1356 (2024)
18. Shurrab, S., Duwairi, R.: Self-supervised learning methods and applications in medical imaging analysis: A survey. *PeerJ Computer Science* **8**, e1045 (2022)
19. Suter, Y., Knecht, U., Valenzuela, W., Notter, M., Hewer, E., Schucht, P., et al.: The lumiere dataset: Longitudinal glioblastoma mri with expert rano evaluation. *Scientific data* **9**(1), 768 (2022)
20. Tang, Y., Yang, D., Li, W., Roth, H.R., Landman, B., Xu, D., et al.: Self-supervised pre-training of swin transformers for 3d medical image analysis. In: Proceedings of the IEEE/CVF conference on computer vision and pattern recognition. pp. 20730–20740 (2022)
21. van der Voort, S.R., Incekara, F., Wijnenga, M.M., Kapsas, G., Gahrmann, R., Schouten, J.W., et al.: The erasmus glioma database (egd): Structural mri scans, who 2016 subtypes, and segmentations of 774 patients with glioma. *Data in brief* **37**, 107191 (2021)

22. Wang, H., Chen, Y., Ma, C., Avery, J., Hull, L., Carneiro, G.: Multi-modal learning with missing modality via shared-specific feature modelling. In: Proceedings of the IEEE/CVF Conference on Computer Vision and Pattern Recognition. pp. 15878–15887 (2023)
23. Wang, Z., Wu, Z., Agarwal, D., Sun, J.: Medclip: Contrastive learning from unpaired medical images and text. In: Proceedings of the Conference on Empirical Methods in Natural Language Processing. Conference on Empirical Methods in Natural Language Processing. vol. 2022, p. 3876 (2022)
24. Weinstein, J.N., Collisson, E.A., Mills, G.B., Shaw, K.R., Ozenberger, B.A., Ellrott, K., et al.: The cancer genome atlas pan-cancer analysis project. *Nature genetics* **45**(10), 1113–1120 (2013)
25. Zhang, Y., He, N., Yang, J., Li, Y., Wei, D., Huang, Y., et al.: mmformer: Multi-modal medical transformer for incomplete multimodal learning of brain tumor segmentation. In: International Conference on Medical Image Computing and Computer-Assisted Intervention. pp. 107–117. Springer (2022)
26. Zhou, L., Liu, H., Bae, J., He, J., Samaras, D., Prasanna, P.: Self pre-training with masked autoencoders for medical image classification and segmentation. In: 2023 IEEE 20th International Symposium on Biomedical Imaging (ISBI). pp. 1–6. IEEE (2023)
27. Zhou, T., Ruan, S., Hu, H.: A literature survey of mr-based brain tumor segmentation with missing modalities. *Computerized Medical Imaging and Graphics* **104**, 102167 (2023)
28. Zhou, Z., Sodha, V., Rahman Siddiquee, M.M., Feng, R., Tajbakhsh, N., Gotway, M.B., et al.: Models genesis: Generic autodidactic models for 3d medical image analysis. In: Medical Image Computing and Computer Assisted Intervention–MICCAI 2019: 22nd International Conference, Shenzhen, China, October 13–17, 2019, Proceedings, Part IV 22. pp. 384–393. Springer (2019)